[5]Pfeifer, H. J., Vom Stein, H. D., and Koch, B., "Mathematical and Experimental Analysis of Light Diffraction on Plane Shock Waves," *Proceedings of the 9th International Congress of High-Speed Photography*, 1970, pp. 423–426.

[6]Born, M., and Wolf, E., *Principles of Optics*, 6th ed., Pergamon, Oxford, England, UK, 1989, p. 425.

Shock Detection Technique Based on Light Scattering by Shock

J. Panda*
University of Toledo, Toledo, Ohio 43606

Introduction

IT has been reported in an accompanying Technical Note[1] that when a narrow laser beam is brought to a grazing incidence on a shock, a small part of the beam scatters out in a thin, diverging sheet of light. The phenomenon disappears when the beam is moved to any other location where there is no shock or the beam pierces the shock surface, i.e., at a nongrazing incidence. Various experimental details indicate that the scattering is primarily due to diffraction of light by the sudden jump in the refractive index created across a shock.

The preceding optical phenomenon is conveniently used as the basis of a new shock detection technique. It depends on moving a laser beam from point to point in a shock-containing flowfield and sensing the presence of the scattered light using a photomultiplier tube (PMT). The incident beam locations, which correspond to a nonzero PMT signal, are the shock locations. It is demonstrated that the present method is able to provide both time-averaged and unsteady information in a very straightforward way.

Experimental Setup

The present experiments were conducted in the shock-containing plume of an underexpanded, supersonic, free jet, exhausted through a 25.4-mm-diam (D) convergent nozzle, at a pressure ratio (plenum pressure/atmospheric pressure) of 3.18 (see Ref. 2). The laser beam used for the detection system is the green line (0.514-μm wavelength) of an argon-ion laser, transmitted by a fiber-optic system. Figure 1 shows a schematic of the setup. The diameter of the beam out of the optical fiber is about 2 mm, which is then focused at the jet centerline to a diameter of 0.16 mm. The setup is similar to the one used for the visualization purpose[1] except for the light collecting and sensing devices. Just in front of the 60-mm-diam collecting lens is a 13-mm-diam beam stop that blocks the main beam. However, the diameter of the beam stop is small enough to allow most of the scattered light to enter the collecting optics. The collecting lens focuses this light to a 0.2-mm-diam pinhole that then passes it to a PMT (TSI model 9162). The electrical output from the PMT is connected across a 50-Ω terminator (not shown in Fig. 1). The voltage drop across the terminator is proportional to the PMT current and, therefore, is an indicator of the intensity of the collected light. The complete optical setup was mounted on a three-axis Klinger traversing unit that allowed it to be moved along the streamwise and the transverse directions within an accuracy of 0.025 mm. Under normal circumstances light from the laser beam does not reach the PMT. However, if the optical arrangement is moved to a location where the laser beam becomes tangential to a shock surface, a part of the scattered light is collected and sensed by the PMT, which then produces a nonzero output. The voltage signal from the PMT was digitized using a dsp Technology sample-and-hold digital converter and then stored and processed by a Microvax 3300 computer.

Received June 9, 1994; revision received Feb. 14, 1995; accepted for publication Feb. 16, 1995.

*Resident Research Associate, Internal Fluid Mechanics Division, NASA Lewis Research Center, Cleveland, OH 44135. Member AIAA.

The detection technique is validated by comparing the shock locations identified by the present optical technique, schlieren photography, and a limited velocity measurement using laser Doppler velocimetry (LDV). The details of the one-component, fiber-optic, dual-beam, forward scatter, LDV system were reported earlier by Panda.[2]

Results

Figure 2 shows a comparison between the shock positions identified using this technique and those seen in a spark-schlieren photograph of the jet. The rms value of the voltage drop across the PMT, measured as the flowfield is surveyed at three radial (z) locations, are shown in Figs. 2b–2d. At $z/D = 0.45$ (close to the shear layer) the schlieren photograph indicates the presence of the shock at an axial location, $x/D = 1.2$ (the markers at the bottom of the schlieren photograph are one jet diameter apart). The laser survey (Fig. 2b) also indicates a large rms voltage around the same axial position. At the other two radial locations, centerline and $z/D = 0.2$, the scattered light is expected to appear twice, since the laser beam becomes tangential to the shock at two locations. First, when it touches the conical shock boundary and second when it touches the base of the cone. At the latter location the shock splits into many "legs" as it ends in the shear layer and any one of these "legs" can be tangential to the laser beam. The laser surveys of Figs. 2c and 2d show large rms voltages exactly around these expected locations as identified from

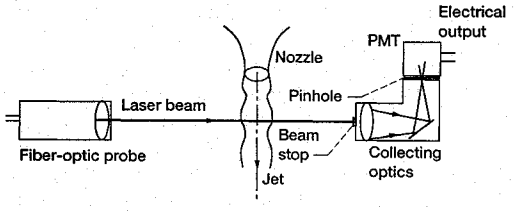

Fig. 1 Schematic of the shock detection technique.

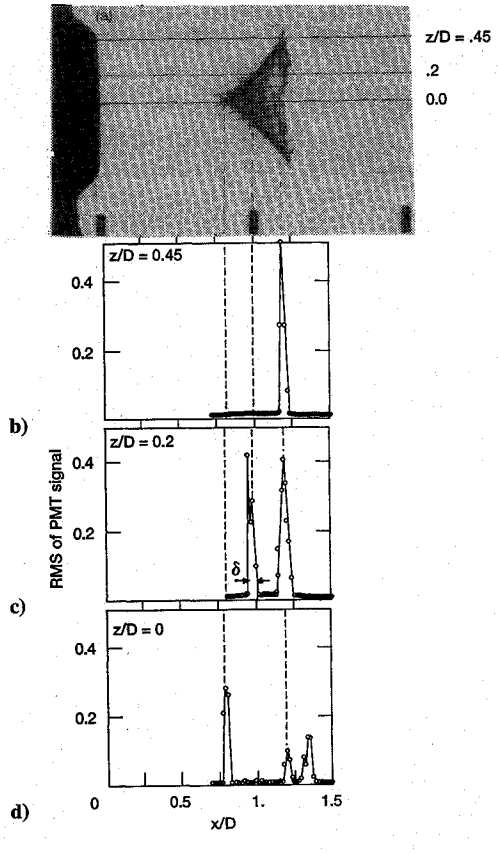

Fig. 2 Validation of the detection technique: a) schlieren photograph of shock formed in underexpanded jet; b), c), and d) laser surveys from indicated radial positions.

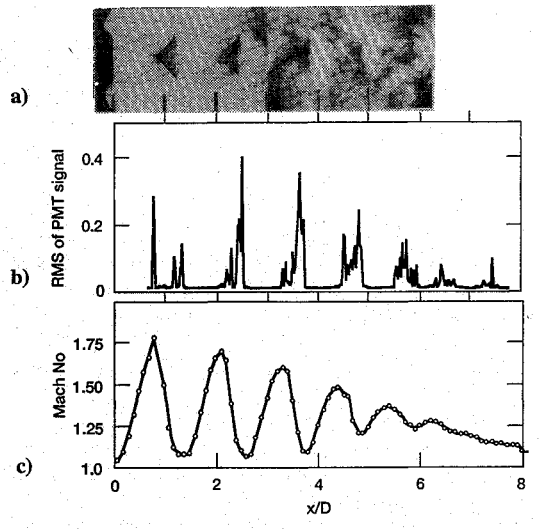

Fig. 3 Validation of the detection technique: a) spark-schlieren photograph, b) laser survey along jet centerline, and c) LDV measurements of centerline Mach number variation.

the schlieren photograph. The third spike in the centerline survey (Fig. 2d) is possibly due to another shock reflected from the shear layer and seen further downstream in the schlieren photograph.

The data shown in Fig. 2 are in the vicinity of the first shock cell only. Similar data for the complete flowfield covering all of the shocks are shown in Fig. 3. This figure also includes the Mach number distribution along the centerline, measured with a laser Doppler velocimetry. The spark-schlieren image (spark duration $\sim 60\ \mu s$) of Fig. 3a is made of two separate photographs, taken at different instances, which are pasted following the marker visible at the bottom. This was necessary due to the small size of the schlieren mirrors (100 mm in diameter).

The centerline shock position data up to $x/D = 1.5$, shown in Fig. 3b, are the same as presented in Fig. 2d. However, a different scale used for the abscissa causes the difference in the appearance. Good agreement can be seen between the shock positions identified in the laser survey (Fig. 3b) and those seen along the centerline of the schlieren photograph (Fig. 3a). The origin of the distinct spikes around the first shock surface is explained earlier. However, the variation of the rms voltage around the subsequent shocks is difficult to explain. It is believed that the large turbulent structures, present in such jets, progressively distort the shocks formed further downstream. Further studies are necessary to understand the distortion and unsteadiness of such shocks.

The purpose of the LDV data of Fig. 3c is to identify the shock locations from the time-averaged velocity measurements. The Mach number distribution, calculated from these data, shows many undulations. The regions over which the local Mach number increases correspond to the expansion regions of the jet and the axial stations where the Mach number starts to drop can be considered as the shock locations. The shock locations indicated from the LDV data match with the corresponding locations indicated by the laser survey. This reconfirms the usefulness of the present optical technique.

Measurement of Shock Unsteadiness

When the laser beam is positioned to touch an oscillatory shock, the scattered light appears periodically, and a time trace obtained from the PMT also shows voltage spikes with the same periodicity.[2] A spectral analysis of the unsteady PMT signal provides the frequency of shock oscillation. Since the response time of a photomultiplier tube is extremely small (on the order of nanoseconds), very high frequency shock motion can be easily detected using this setup. Figure 4a presents two spectra of the PMT signal when the laser beam was positioned individually on the first two shock surfaces in the underexpanded jet. For a comparison, an acoustic spectrum, measured using a microphone placed near the jet, is also shown in Fig. 4b. The peaks seen in the acoustic spectrum correspond to the screech frequency and a few of its harmonics. All such peaks are also present in the shock motion spectra of Fig. 4a, which indicate that

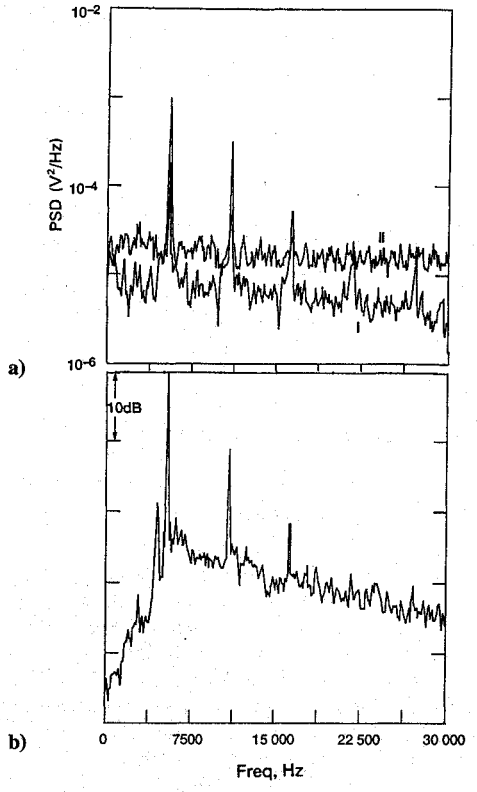

Fig. 4 Comparison between shock unsteadiness and sound spectrum: a) spectra of the PMT signal from indicated shocks, $z/D = 0.15$; and b) acoustic spectrum from nozzle lip.

each shock oscillates at the frequency of the emitted sound. This observation is supported by an earlier experiment of Lassiter and Hubbard,[3] who photographed shadowgraph images of the jet using a high-speed movie camera to determine the frequency of shock motion (also see Norum and Seiner[4]). It is worth mentioning here that the technique is also useful in providing statistics, like the PDF of shock position, for flows involving aperiodic shock motion.

In addition to the frequency information, the amplitude of shock oscillation can also be determined by using the present shock detection scheme. For this purpose, the flowfield has to be scanned by the laser beam at closely spaced points over the distance through which the shock is expected to move. The spatial extent over which a nonzero value of the time-averaged PMT voltage is obtained represents the amplitude of the oscillating shock. This is best demonstrated through Fig. 2, where data from laser surveys around the first shock surface are presented. For every encounter with the shock surface, a high value of the PMT voltage is obtained over a spatial extent shown as δ in Fig. 2c. The average width of all of such δ in Figs. 2b–2d is measured to be 0.067D (1.7 mm), which represents the average amplitude of oscillation of the first shock surface. The accuracy of the measurement is limited by the laser beam diameter, 0.16 mm for the present case.

Concluding Remarks

The primary advantage of the current method over a quantitative schlieren or shadowgraph system lies in its simplicity and accessibility. The large schlieren mirrors and other accessories are difficult to use in a complex flow geometry, such as a turbomachinery flow passage. The present method, on the other hand, depends on a narrow laser beam that is far more accessible and can be used much more conveniently in complex geometries. Perhaps, the best use of this technique is in measuring unsteady shock motion where statistics, such as amplitude, frequency, and probability density function of shock position, can be obtained in a very straightforward way.

Acknowledgment

The author acknowledges the helpful discussions with K. B. M. Q. Zaman of NASA Lewis on shock oscillation.

References

[1]Panda, J., "Wide Angle Light Scattering in Shock-Laser Interaction," *AIAA Journal*, Vol. 33, No. 12, pp. 2429–2431.

[2]Panda, J., "Partial Spreading of a Laser Beam into a Light Sheet by Shock Waves and Its Use as a Shock Detection Technique," NASA CR-195329, May 1994.

[3]Lassiter, L. W., and Hubbard, H. H., "The Near Noise Field of Static Jets and Some Model Studies of Devices for Noise Reduction," NACA TN 3187, July 1954.

[4]Norum, T. D., and Seiner, J. M., "Location and Propagation of Shock Associated Noise from Supersonic Jets," AIAA Paper 80-0983, June 1980.

Stress and Failure Analysis for Cross-Plied Curved Composite Laminates

Naoyuki Watanabe*
Tokyo Metropolitan Institute of Technology, Tokyo 191, Japan
and
Takao Okada†
National Aerospace Laboratory, Tokyo 182, Japan

I. Introduction

MANY laminated composite structures that have a curved portion, such as an angle bracket, a co-curved web, or a frame, are used for aerospace structures,[1] because design requirements often necessitate the use of complex geometries in the fabrication of load-bearing components. In such curved portions, a tensile radial stress happens under some loading conditions.[2–4] In the curved region of a laminated structure, two major modes of failure were observed, i.e., transverse matrix cracking due to bending stress and interlaminar delamination due to high interlaminar normal stress in the thickness direction. If delamination occurs first, then a total failure, i.e., final failure, of the structure results. However, the structure usually can sustain additional loading after initial transverse matrix cracking. Under increasing loading, these matrix cracks would cause delaminations that would lead to the total collapse of the structure.[2,4,5] Thus, a delamination between layers may be caused by the interlaminar normal stress in the middle region of such laminate far from its free edge, whereas in a flat laminate it always begins to expand necessarily from a free edge. Therefore, for investigating the strength of curved laminates the radial stress must be evaluated accurately.

In this paper, cross-plied curved composite laminates are analyzed for stress and failure using the two-dimensional finite element method (FEM). The strength for in-plane failure of each layer is predicted using the Tsai–Wu criterion, and the maximum radial stress criterion is used for a delamination. These two strengths are investigated for various lay-ups. The three-dimensional FEM is carried out for indicating the validity of the two-dimensional FEM.

II. Effect of Stacking Sequence on the Strength of Cross-Plied Curved Composite Laminate

The effect of the stacking sequence on the strength of cross-plied curved composite laminates shown in Fig. 1 is evaluated. Plane stress state on the x–y plane is assumed and the two-dimensional FEM is carried out. The material constants, the strength properties, and the dimensional parameters are assumed here as follows:

$$L_p = 10 \text{ mm}, \quad L_h = 10 \text{ mm}, \quad R_0 = 8 \text{ mm}$$
$$R_i = 5 \text{ mm}, \quad t = 3 \text{ mm}, \quad E_L = 140 \text{ GPa}, \quad E_T = 11 \text{ GPa}$$
$$G_{LT} = 5.84 \text{ GPa}, \quad G_{TT} = 4.44 \text{ GPa}, \quad \nu_{LT} = 0.3$$
$$\nu_{TT} = 0.28, \quad F_{Lt} = 1.50 \text{ GPa}, \quad F_{Lc} = 1.00 \text{ GPa}$$
$$F_{Tt} = 0.0685 \text{ GPa}, \quad F_{Tc} = 0.194 \text{ GPa}, \quad F_{LT} = 0.115 \text{ GPa}$$

One of the strengths is concerned with the in-plane failure of each layer, and it is assumed to be estimated by means of the Tsai–Wu criterion.[6,7] The coefficient F_{12}^* used in it is assumed to be -0.5 according to Ref. 10. The other strength is related to the delamination on the interface between two adjacent layers and is estimated as follows:

$$\sigma_r \geq F_{Tt} \tag{1}$$

Although the delamination strength isn't the same for each interface of 0/0, 0/90, and 90/90 deg, the exact values are not known, so the preceding assumption is done in this paper also.[2,5] As typical stacking sequence, six are carried out

$$\text{L1: } [0_4/90_3/0_5]_{\text{sym}}, \quad \text{L2: } [0_7/90_3/0_2]_{\text{sym}}, \quad \text{L3: } [0_2/90_3/0_7]_{\text{sym}}$$
$$\text{L4: } [0_9/90_3]_{\text{sym}}, \quad \text{L5: } [0_2/90_{10}]_{\text{sym}}, \quad \text{L6: } [0_4/90_3/0_6/90_3/0_8]$$

where the stacking sequence is written from its inside and the 0-deg layer means that fibers go on the x–y plane along its arc and the 90-deg layer means that they go along the out-of-plane direction, i.e., z direction.

Table 1 shows the results under the upward external load. The magnitude of the load when the failure mode begins to occur, the angle of circular arc, and the layer number of the location where the failure occurs are shown in the table. For delamination, the location of the interface is written.

From comparing L1 with L2, it is shown that the shift of 90-deg plies to the middle increases the in-plane failure strength with a

Table 1 Failure loads for in-plane failure and interlaminar delamination together with location where its failure occurs under upward external load for various lay-ups

	In-plane failure			Delamination		
		Location			Location	
Lay-up	Load, N/mm	Angle, deg	Layer[a]	Load, N/mm	Angle, deg	Interface[b]
L1	44.0	15	5 (90)	61.1	25	10 (0), 11 (0)
L2	48.2	25	8 (90)	58.1	19	7 (0), 8 (90)
L3	39.7	15	3 (90)	56.5	25	10 (0), 11 (0)
L4	51.6	25	10 (90)	58.3	19	9 (0), 10 (90)
L5	31.2	15	3 (90)	64.9	15	3 (90), 4 (90)
L6	45.5	15	5 (90)	62.4	25	10 (0), 11 (0)

[a]Number of layers from its inside, and the figure in parentheses indicates the fiber angle.
[b]Interface between two layers.

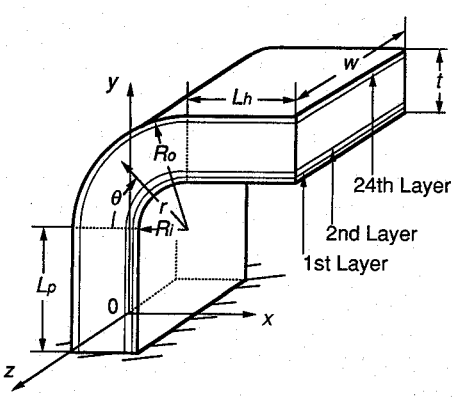

Fig. 1 Cross-plied laminate with a quarter of circular arc.

Presented as Paper 93-1519 at the AIAA/ASME/ASCE/AHS/ASC 34th Structures, Structural Dynamics, and Materials Conference, La Jolla, CA, April 19–22, 1993; received Dec. 14, 1993; revision received March 20, 1995; accepted for publication Aug. 10, 1995.

*Associate Professor, Department of Aerospace Engineering, 6-6, Asahigaoka, Hino-Shi. Member AIAA.

†Researcher, Structural Mechanics Division, 7-44-1, Jindaiji Higashimachi, Chofu-shi.